Dalton Transactions

An international journal of inorganic chemistry

rsc.li/dalton

ROYAL SOCIETY
OF **CHEMISTRY**
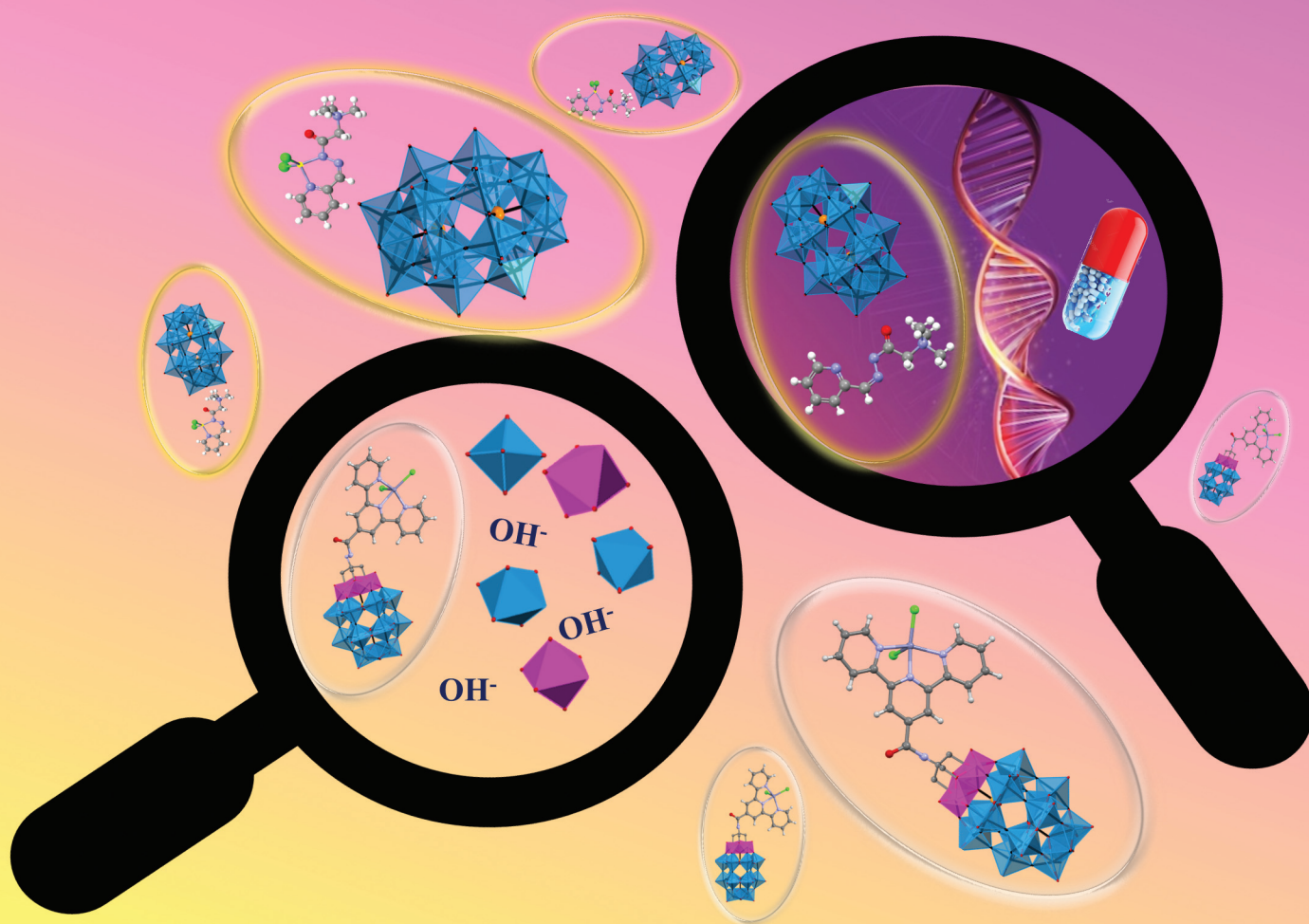
PAPER
Marta Fik-Jaskółka, Adam Gorczyński *et al.*
The effect of ionic *versus* covalent functionalization of
polyoxometalate hybrid materials with coordinating subunits
on their stability and interaction with DNA

Check for updates

The effect of ionic *versus* covalent functionalization of polyoxometalate hybrid materials with coordinating subunits on their stability and interaction with DNA†

Daria Nowicka,‡[a] Dawid Marcinkowski, [iD] ‡[a] Nahir Vadra, [iD] [b] Martyna Szymańska,[a] Maciej Kubicki, [iD] [a] Giuseppe Consiglio,[c] Wojciech Drożdż,[a,d] Artur R. Stefankiewicz, [iD] [a,d] Violetta Patroniak, [iD] [a] Marta Fik-Jaskółka [iD] *[a] and Adam Gorczyński [iD] *[a]

Inorganic–organic hybrid materials that combine both Polyoxometalates (POMs) and metal ion coordinating subunits (CSUs) represent promising multifunctional materials. Though their individual components are often biologically active, utilization of hybrid materials in bioassays significantly depends on the functionalization method and thus resulting stability of the system. Quite intriguingly, these aspects were very scarcely studied in hybrid materials based on the Wells–Dawson POM (WD POM) scaffold and remain unknown. We chose two model WD POM hybrid systems to establish how the functionalization mode (ionic *vs.* covalent) affects their stability in biological medium and interaction with nucleic acids. The synthetic scope and limitations of the covalent POM-terpyridine hybrids were demonstrated and compared with the ionic Complex-Decorated Surfactant Encapsulated-Clusters (CD-SECs) hybrids. The nature of POM and CSU binding can be utilized to modulate the stability of the hybrid and the extent of DNA binding. The above systems show potential to behave as model cargo-platforms for potential utilization in medicine and pharmacy.

Introduction

Polyoxometalates (POMs) can be described as a group of transition metals in their highest oxidation state linked together by oxygen atoms with a general formula $[MO_x]_n$, where M = Mo, W, V, and Nb, and $x = 4$–7,[1–3] which can form different structures of varying sizes by gradual condensation. Besides, heteroatoms such as P, Si, Al, or S and transition metal ions

[a]*Adam Mickiewicz University in Poznań, Faculty of Chemistry, Uniwersytetu Poznańskiego 8, 61-614 Poznań, Poland. E-mail: marta.fik@amu.edu.pl, adam.gorczynski@amu.edu.pl*
[b]*Universidad de Buenos Aires, Facultad de Ciencias Exactas y Naturales, Departamento de Química Inorgánica, Analítica y Química Física and CONICET–Universidad de Buenos Aires, Instituto de Química Física de los Materiales, Medio Ambiente y Energía (INQUIMAE), Buenos Aires C1428EGA, Argentina*
[c]*Università di Catania, Dipartimento di Scienze Chimiche, I-95125 Catania, Italy*
[d]*Adam Mickiewicz University in Poznań, Center for Advanced Technology, Uniwersytetu Poznańskiego 10, 61-614 Poznań, Poland*
†Electronic supplementary information (ESI) available: Spectroscopic analysis of synthesized hybrids and chosen biological spectra. CCDC 2078396. For ESI and crystallographic data in CIF or other electronic format see DOI: https://doi.org/10.1039/d4dt00965g
‡Equal contribution.

such as Co, Fe, Ni, Cu, Zn, or Ln may be present, resulting in more stable systems commonly named as archetypical groups as *e.g.*, Keggin, Wells Dawson (WD), Anderson or Preyssler.[4] In addition, vacancies in the structure can be generated by controlled hydrolysis (*e.g.*, lacunary POMs), giving new reactive centers that can be linked using electrophiles to form larger aggregates or utilized for postfunctionalization.[5,6] Given their anionic characteristics, POMs can also bind different cations,[7] and the final architecture and the physicochemical properties of the complex formed depend on the participating components of the complex.[8]

Self-assembly and functionalization processes in POMs are not always straight-forward, and they are highly influenced by small changes in reaction conditions such as pH, temperature or stoichiometry and therefore, it is not always easy to predict the architecture and have a preprogrammed design.[4] In the last few years, there have been numerous efforts to find new approaches to control the structure of POMs, some of the reported strategies have pointed to controlling self-assembly using classical approaches (such as trapping of functional metallic cores, molecular nanoparticles, or incorporation of active sites),[8] while the latest ones focus on using Machine learning[9] and automated chemistry.[10]

The versatility and variety of properties in these systems have led in the recent years to exploring ways to diversify the physicochemical properties, for example, by generating hybrid inorganic–organic architectures.[11] In general terms, hybrid inorganic–organic POMs may be obtained by different approaches such as (1) nanostructurization of small POMs into larger ones;[12] (2) covalent linking of organic moieties onto the POM cluster surface;[13] (3) non-covalent functionalization (ionic interaction or hydrogen bonding) through the formation of the Surfactant-Encapsulated-Clusters (SECs).[13] We have also presented a new pathway (4) to generate a novel family POMs inorganic–organic systems to form Complex-Decorated Surfactant-Encapsulated-Cluster (CD-SEC) materials.[14] It is a multilevel functionalization based on the decoration of WD POMs with organic cation surfactant, which could simultaneously act as a metal ion complexing agent allowing for high versatility and tunable functionality. As a result, extensive exploration has been carried out for those systems concerning applications in fields such as catalysis,[15,16] electrocatalysis,[17,18] hydrogen generation,[19] protein crystallography,[20] elaboration of functional materials.[21–23]

Biological applications are also promising in terms of the potential of POMs to modify and enhance interaction with biomacromolecules.[24–26] Indeed, a high negative charge accompanied by a large number of oxo-ligands results in POMs that can be treated as water-soluble macroanions, thus representing perfect models for studying the biomacromolecular interactions in polyelectrolyte solutions.[27] Iso and heteropolyanions were studied in terms of hydrolytic cleavage of peptides,[28] nucleotides,[29] and saccharides,[30] along with analysis of the POM-biomolecule mechanisms that govern the observed outcomes.[31] Consequently, systematic studies on potential applications, such as antiviral,[32] antidiabetic,[33] antibiotic[34] or anticancer[35] effects, have been reported. Nevertheless, high toxicity in normal cells and unclear biochemical pathways indicate the need for further studies. Recently recognized organic–inorganic hybrid systems have been shown to enhance the anticancer activity[35] and exhibit more effective antibacterial properties than the inorganic analogues.[34] Both derivatization with organic moieties *via* covalent bonds and their encapsulation inside non-toxic organic macromolecules could lead to systems with enhanced biocompatibility, higher stability at physiological pH and lower toxicity.[36–39] However, these results are still scarcely understood, and the need to construct such systems and studies is therefore justified.

Herein, we have chosen WD POMs to study due to their ability to undergo a variety of modifications and formation of organic–inorganic hybrids that exhibit potential biological activity. In this work we have studied how the ionic *vs.* covalent functionalization of the hybrid WD POM based system affects their stability in the presence of DNA and interacts with this biological system. To establish this, two distinct systems were preprogrammed: (i) previously demonstrated CD-SECs; (ii) covalently bound POM-tpy, and chosen, together with the construction algorithms that demonstrate the potential feasibility of such systems, to act as the drug carrier models.

Experimental section

Materials and methods

The metal salts, organic compounds and solvents were supplied by Aldrich and POCH. All chemicals mentioned above were of analytical grade quality and were used as obtained without further purification. The precursor **V$_3$POM-TBA** TBA$_5$H$_4$[P$_2$W$_{15}$V$_3$O$_{62}$] POM was synthesized and characterized following published procedures (K$_6$[α-P$_2$W$_{18}$O$_{62}$]·14H$_2$O^{40} → Na$_{12}$[α-P$_2$W$_{15}$O$_{56}$]·18H$_2$O^{41} → K$_8$H[P$_2$W$_{15}$V$_3$O$_{62}$]·9H$_2$O^{42} → TBA$_5$H$_4$[P$_2$W$_{15}$V$_3$O$_{62}$]).[42]

V$_3$POM + TRIZMA (TBA)$_4$H$_2$[H$_2$NC(CH$_2$O)$_3$P$_2$V$_3$W$_{15}$O$_{59}$]· 3C$_3$H$_7$NO was synthesized following published procedure.[43] All reactions were performed under an argon atmosphere condition unless otherwise stated with magnetic stirring and in the dark to prevent photoreduction of the V^{5+} containing POM to mixed valence V^{5+}/V^{-4+} POMs. Ligand **L^{tpy}** was obtained according to the previously reported procedure.[44] IR spectra were obtained with a PerkinElmer 580 spectrophotometer and peak positions are reported in cm^{-1}. ESI mass spectra were determined in methanolic solution with c = ~10^{-4} M using a Waters Micromass ZQ spectrometer. NMR spectra were run on a Varian VNMR-S 400 MHz spectrometer and were calibrated against the residual protonated solvent signals (DMSO-d_6, δ 2.50; D$_2$O, δ 3.33) which are given in parts per million. In ^{31}P NMR 25% H$_3$PO$_4$ was used as an external reference. Electronic absorption titrations and stability tests of compounds were performed on JASCO V-770 spectrophotometer equipped with a Peltier PAC-743R at a temperature of 20 °C in 10 × 10 mm quartz cells in the range of 800–200 nm. pH measurements were tested on Mettler Toledo Seven Compact S210 pH meter.

Synthetic procedure of complex K1 [Zn(L^{tpy})Cl$_2$]

Ligand **L^{tpy}** (100.0 mg, 0.30 mmol) was placed in a 50 ml round-bottom flask and dissolved in the mixture methanol/acetonitrile (1 : 1, v : v) (10 ml). The ZnCl$_2$ (40.9 mg, 0.30 mmol) was dissolved in a mixture of methanol/acetonitrile (1 : 1, v : v) (10 ml). Then the salt solution was added to the ligand and the solution changed colour from transparent to light yellow. The resulting mixture was stirred for 24 hours at room temperature. After this time, the reaction mixture was evaporated to dryness under reduced pressure. The residue was dissolved in a minimal amount of methanol/acetonitrile (1 : 1, v : v) (*ca.* 1 ml) and precipitated by the adding an excess of diethyl ether (approx. 30 ml). The resulting white precipitate was filtered off with suction and dried in a vacuum. Yield: 80.0 mg, 57.0%. ESI-MS(+) m/z (%): 335 (100) [**L^{tpy}** + H]$^+$, 433 (30) [ZnL^{tpy}Cl]$^+$. Anal. calc.: C, 51.15; H, 4.08; N, 8.95; found: C, 51.05; H, 3.98; N, 9.02%. IR (KBr, cm^{-1}): ν(C–H)$_{ar}$ 3392; ν_s(CH$_3$) 2449; ν(C=O) 1627; ρ(C–H)$_{ar}$1040; γ(C–H)$_{ar}$ 553. ^{1}H NMR (400 MHz, DMSO-d_6): δ = 9.06 (s, 1H), 8.71 (d, J = 7.9 Hz, 1H), 8.17 (t, J = 7.8 Hz, 1H), 7.69 (d, J = 7.7 Hz, 1H), 4.58–4.45 (m, 1H), 3.01 (s, 4H), 1.46 (t, J = 7.1 Hz, 2H). Solubility problems result in a mixture of "open" (metal ion : ligand; 1 : 1) and "closed" (metal ion : ligand; 1 : 2) systems.

Synthetic procedure of complex K2 [Zn(L^{tpy})$_2$](ClO$_4$)$_2$

Ligand L^{tpy} (100.0 mg, 0.30 mmol) was placed in a 50 ml round-bottom flask and dissolved in the mixture methanol/acetonitrile (1 : 1, v : v) (10 ml). The Zn(ClO$_4$)$_2$·6H$_2$O (55.9 mg, 0.15 mmol) was dissolved in a mixture of methanol/acetonitrile (1 : 1, v : v) (10 ml). Then the salt solution was added to the ligand solution. The resulting transparent mixture was stirred for 24 hours at room temperature. After this time, the reaction mixture was evaporated to dryness under reduced pressure. The residue was dissolved in a minimal amount of methanol/acetonitrile (1 : 1, v : v) (about 1 ml) and precipitated by adding an excess of diethyl ether (approx. 30 ml). The resulting white precipitate was filtered off with suction and dried in a vacuum. White solid residue was recrystallized by slow diffusion method from diisopropyl ether into methanol/acetonitrile (1 : 1, v : v) system at lowered temperature. Yield: 105.0 mg, 75.0%. ESI-MS(+) m/z (%): 335 (30) [L^{tpy} + H]$^+$, 356 (50) [L^{tpy} + Na]$^+$, 366 (80) [ZnL^{tpy}_2]$^{2+}$, 831 (10) [ZnL^{tpy}_2(ClO4)]$^+$. IR (KBr, cm^{-1}): ν(C–H)$_{ar}$ 3104; ν_s(CH$_3$) 2980, 2931; ν(C=O) 1773; ν(C=C)$_{ar}$ 1604, 1570, 1478, ν(C–N) 1442, 1372; ν(C=N)$_{ar}$ 1269, 1249; ρ(C–H)$_{ar}$ 1139, 1089; γ(C–H)$_{ar}$ 810, 769, 740; γ(ClO) 622. ^{1}H NMR (400 MHz, DMSO-d_6): δ = 8.82 ppm (s, 2H), 8.44 ppm (d, 2H), 7.91 ppm (t, 2H), 7.40 ppm (d, 2H), 4.46 ppm (q, 2H), 2.62 ppm (s, 6H), 1.40 ppm (t, 3H).

Synthetic procedure of hybrid H1^{cov} (POM + L^{tpy}) [V$_3$POM + TRIZMA + L^{tpy}]TBA$_6$

V$_3$POM + TRIZMA (50 mg, 0.01 mmol) was dissolved in 15 ml of acetonitrile and added to a two necked 50 ml flask equipped with a condenser. Ligand L^{tpy} (3.2 mg, 0.01 mmol) was dissolved in 5 ml of acetonitrile and was added to solution of V$_3$POM + TRIZMA. The solution changed colour from brown-orange to yellow-green. Then the mixture was heated under reflux for 3 days. The resulting yellow-green precipitate was filtered off with suction, washed with acetonitrile and dried in a vacuum. Yield: 41.5 mg, 78.0%. ESI-MS(−) m/z (%): 716 (20) [L^{tpy}(V$_3$POM + trizma)]$^{6-}$. Anal. calc.: C, 25.03; H, 4.25; N, 2.43; found: C, 25.01; H, 4.31; N, 2.38%. IR (KBr, cm^{-1}): ν(N–H) 3446; ν_s(CH$_3$) 2932, 2872; ν(C=O) 1633; ν(C–N) 1465, 1379; ρ(C–H)$_{ar}$ 1086; γ(C–H)$_{ar}$ 952, 910, 817, 528. ^{1}H NMR (400 MHz, DMSO-d_6): δ = 8.85 ppm (s, 2H, HL), 8.49 ppm (d, 2H, HL), 7.99 ppm (m, 2H, HL), 7.46 ppm (d, 2H, HL), 5.39 ppm (s, 6H, O-CH$_2$-C), 3.16 ppm (m, 48H, HTBA), 2.65 ppm (s, 6H, HL), 1.57 ppm (p, 48H, HTBA), 1.31 ppm (h, 48H, HTBA), 0.98 ppm (t, 72H, HTBA). ^{31}P NMR (162 MHz, DMSO-d_6): δ = −6.65 ppm, −12.70 ppm.

Synthetic procedure of hybrid H2^{cov} (POM + K1) [Zn(V$_3$POM + TRIZMA + L^{tpy})Cl$_2$]TBA$_6$

V$_3$POM + TRIZMA (50 mg, 0.01 mmol) was dissolved in 8 ml of acetonitrile and added to two necked 50 ml flask. K1 (4.5 mg, 0.01 mmol) was added to solution of V$_3$POM + TRIZMA. The homogeneous mixture was heated under reflux for 24 hours. After this time clear yellow solution was condensed on rotavapor and diethyl ether was added. The resulting yellow precipi-

tate was centrifuged, washed with diethyl ether and dried in a vacuum. Yield: 50.8 mg, 87.6%. ESI-MS(−) m/z (%): 962 (30) [L^{tpy}(V$_3$POM + trizma)Cl + 2TBA]$^{5-}$, 1638 (40) [Zn L^{tpy}(V$_3$POM + trizma)Cl$_2$ + H + 2TBA]$^{3-}$. Anal. calc.: C, 25.45; H, 4.15; N, 2.38; found: C, 25.58; H, 4.21; N, 2.31%. IR (KBr, cm^{-1}): ν(N–H) 3436; ν_s(CH$_3$) 2963, 2873; ν(C=O) 1644; ν(C–N) 1473, 1391; ρ(C–H)$_{ar}$ 1079; γ(C–H)$_{ar}$ 952, 900, 804, 737, 514. ^{1}H NMR (400 MHz, DMSO-d_6): δ = 8.84 ppm (s, 2H, H$_L$), 8.38 ppm (s, 2H, H$_L$), 7.95 ppm (s, 2H, H$_L$), 7.28 ppm (s, 2H, H$_L$), 5.39 ppm (s, 6H, O-CH$_2$-C), 3.17 ppm (t, 48H, H$_{TBA}$), 2.59 ppm (s, 6H, H$_L$), 1.56 ppm (p, 48H, H$_{TBA}$), 1.23 ppm (h, 48H, H$_{TBA}$), 0.94 ppm (t, 72H, H$_{TBA}$). ^{31}P NMR (162 MHz, DMSO-d_6): δ = −6.65 ppm, −12.70 ppm.

Synthetic procedure of hybrid H3^{cov} (POM + K2) [Zn(V$_3$POM + TRIZMA + L^{tpy})$_2$(ClO$_4$)$_2$]TBA$_{(12-x)}$H$_x$; x = 11.5

V$_3$POM + TRIZMA (100 mg, 0.02 mmol) was dissolved in 15 ml of acetonitrile and added to two necked 50 ml flask. K2 (7.0 mg, 0.01 mmol) was added to solution of V$_3$POM + TRIZMA. The heterogeneous mixture was heated under reflux for 24 hours. After this time a clear yellow solution was condensed on a rotavapor and placed at 4° deg overnight. The resulting yellow precipitate was filtered off with suction, washed with acetonitrile and dried in a vacuum. Yield: 38.0 mg, 71.7%. ESI-MS(−) m/z (%): 795 (30) [Zn(L^{tpy}(V$_3$POM + trizma))$_2$ClO$_4$]$^{11-}$, 1089 (70) [ZnL^{tpy}(V$_3$POM + trizma)]$^{4-}$. IR (KBr, cm^{-1}): ν(N–H) 3465; ν_s(CH$_3$) 2952, 2863; ν(C=O) 1629; ν(C=C)$_{ar}$ 1570; ν(C–N) 1458, 1384; ν(C=N)$_{ar}$ 1272; ρ(C–H)$_{ar}$ 1079; γ(C–H)$_{ar}$ 975, 900, 818, 730, 514. ^{1}H NMR (400 MHz, DMSO-d_6): 8.85 ppm (s, 4H, H$_L$), 8.50 ppm (d, 4H, H$_L$), 7.99 ppm (m, 4H, H$_L$), 7.48 ppm (d, 4H, H$_L$), 5.40 ppm (s, 6H, O-CH$_2$-C), 3.16 ppm (m, 3H, H$_{TBA}$), 2.65 ppm (s, 12H, H$_L$), 1.57 ppm (s, 3H, H$_{TBA}$), 1.30 ppm (p, 3H, H$_{TBA}$), 0.93 ppm (t, 5H, H$_{TBA}$). ^{31}P NMR (162 MHz, DMSO-d_6): δ = −6.65 ppm, −12.70 ppm.

Synthetic procedure of hybrid H4^{cov} (H1^{cov} + ZnCl$_2$) [Zn (V$_3$POM + TRIZMA + L^{tpy})Cl$_2$]H$_2$TBA$_4$

Hybrid H1^{cov} (30 mg, 0.005 mmol) was dissolved in 5 ml of acetonitrile and added to two necked 50 ml flask. Next, solution of ZnCl$_2$ (0.7 mg, 0.005 mmol) was added to solution of hybrid H1^{cov}. The heterogeneous mixture was heated under reflux for 24 hours. After this time the solution changed colour from violet to grey-green. The mixture was condensed on rotavapor and diethyl ether was added. The resulting grey-green precipitate was filtered via suction filtration, washed with diethyl ether and dried in a vacuum. Yield: 21.0 mg, 43.9%. ESI-MS(−) m/z (%): 915 (20) [L^{tpy}(V$_3$POM + trizma)Cl + H + TBA]$^{5-}$, 1204 (10) [L^{tpy}(V$_3$POM + trizma)Cl + H + 2TBA]$^{4-}$. Anal. calc.: C, 19.53; H, 3.22; N, 2.07; found: C, 19.75; H, 3.29; N, 2.10%. IR (KBr, cm^{-1}): ν(N–H) 3443; ν_s(CH$_3$) 2960, 2878; ν(C=O) 1644; ν(C–N) 1466, 1377; ν(C=N)$_{ar}$ 1272; ρ(C–H)$_{ar}$ 1087; γ(C–H)$_{ar}$ 952, 915, 812, 722, 536. ^{1}H NMR (400 MHz, DMSO-d_6): δ = 8.85 ppm (s, 2H, H$_L$), 8.48 ppm (d, 2H, H$_L$), 7.96 ppm (m, 2H, H$_L$), 7.45 ppm (d, 2H, H$_L$), 5.39 ppm (s, 6H, O-CH$_2$-C), 3.16 ppm (t, 32H, H$_{TBA}$), 2.64 ppm (s, 6H, H$_L$),

1.56 ppm (p, 32H, H_{TBA}), 1.32 ppm (h, 32H, H_{TBA}), 0.94 ppm (t, 48H, H_{TBA}). ^{31}P NMR (162 MHz, DMSO-d_6): $\delta = -6.65$ ppm, -12.70 ppm.

Synthetic procedure of hybrid H5^{cov} (H1^{cov} + Zn(ClO$_4$)$_2$) [Zn(V$_3$POM + TRIZMA + L^{tpy})$_2$(ClO$_4$)$_2$]H$_{12}$

Hybrid **H1^{cov}** (30 mg, 0.005 mmol) was dissolved in 5 ml of acetonitrile and added to two necked 50 ml flask. Next, **Zn(ClO$_4$)$_2$·6H$_2$O** (1.0 mg, 0.0026 mmol) was added to solution of hybrid **H1^{cov}**. The heterogeneous mixture was heated under reflux for 24 hours. The resulting yellow precipitate was centrifuged, washed with acetonitrile and dried in a vacuum. Yield: 25.8 mg, 98.7%. ESI-MS(−) m/z (%): 575 (10) [L^{tpy}(V$_3$POM + trizma)(ClO$_4$)$_3$ + H]$^{8-}$, 604 (30) [L^{tpy}(V$_3$POM + trizma)(ClO$_4$)$_3$ + TBA]$^{8-}$. IR (KBr, cm^{-1}): ν(N–H) 3465; ν_s(CH$_3$) 2982, 2915; ν(C=O) 1607; ν(C=C)$_{ar}$ 1540; ν(C–N) 1435, 1391; ν(C=N)$_{ar}$ 1287; ρ(C–H)$_{ar}$ 1087; γ(C–H)$_{ar}$ 960, 900, 797, 722, 522. ^1H NMR (400 MHz, DMSO-d_6): 8.85 ppm (s, 4H, H_L), 8.48 ppm (d, 4H, H_L), 7.97 ppm (m, 4H, H_L), 7.45 ppm (d, 4H, H_L), 5.39 ppm (s, 12H, O-CH$_2$-C), 2.64 ppm (s, 12H, H_L). ^{31}P NMR (162 MHz, DMSO-d_6): $\delta = -6.67$ ppm, -12.70 ppm.

Synthetic procedure of hybrid H6^{cov} (POM + L^{tpy} + ZnCl$_2$) [Zn(V$_3$POM + TRIZMA + L^{tpy})Cl$_2$]TBA$_{(6-x)}$H$_x$; x = 5.75

V$_3$POM + TRIZMA (50 mg, 0.01 mmol) was dissolved in 8 ml of acetonitrile and added to two necked 50 ml flask. **L^{tpy}** (3.2 mg, 0.01 mmol) and **ZnCl$_2$** (1.3 mg, 0.01 mmol) were added to solution of **V$_3$POM + TRIZMA**. The mixture changed colour to dark violet. The heterogeneous mixture was heated under reflux for 24 hours. After 3 hours the mixture turned yellow again. The resulting gray-green precipitate was centrifuged, washed with acetonitrile and dried in a vacuum. Yield: 17.4 mg, 36.4%. ESI-MS(−) m/z (%): 962 (30) [L^{tpy}(V$_3$POM + trizma)Cl + 2TBA]$^{5-}$, 1089 (30) [Zn L^{tpy}(V$_3$POM + trizma)]$^{4-}$. Anal. calc.: C, 6.48; H, 0.75; N, 1.26; found: C, 6.51; H, 0.80; N, 1.31%. IR (KBr, cm^{-1}): ν(N–H) 3458; ν(C–H)ar 3086; ν_s(CH$_3$) 2960, 2863; ν(C=O) 1636; ν(C=C)$_{ar}$ 1577, 1517; ν(C–N) 1428, 1384; ν(C=N)$_{ar}$ 1265; ρ(C–H)$_{ar}$ 1071; γ(C–H)$_{ar}$ 960, 908, 812, 737, 522. ^1H NMR (400 MHz, DMSO-d_6): δ = 8.85 ppm (s, 2H, H_L), 8.50 ppm (d, 2H, H_L), 7.98 ppm (d, 2H, H_L), 7.49 ppm (d, 2H, H_L), 5.40 ppm (s, 6H, O-CH$_2$-C), 3.16 ppm (m, 2H, H_{TBA}), 2.66 ppm (s, 6H, H_L), 1.57 ppm (p, 2H, H_{TBA}), 1.31 ppm (h, 2H, H_{TBA}), 0.94 ppm (t, 3H, H_{TBA}). ^{31}P NMR (162 MHz, DMSO-d_6): $\delta = -6.65$ ppm, -12.70 ppm.

Synthetic procedure of hybrid H7^{cov} (POM + L^{tpy} + Zn(ClO$_4$)$_2$) [Zn(V$_3$POM + TRIZMA + L^{tpy})$_2$(ClO$_4$)$_2$]TBA$_{(12-x)}$H$_x$; x = 11.5

V$_3$POM + TRIZMA (50 mg, 0.01 mmol) was dissolved in 8 ml of acetonitrile and added to two necked 50 ml flask. **L^{tpy}** (3.2 mg, 0.01 mmol) and **Zn(ClO$_4$)$_2$·6H$_2$O** (1.8 mg, 0.005 mmol) were added to solution of **V$_3$POM + TRIZMA**. The heterogeneous mixture was heated under reflux for 24 hours. The resulting yellow precipitate was centrifuged, washed with acetonitrile and dried in a vacuum. Yield: 34.3 mg, 64.7%. ESI-MS(−) m/z (%): 716 (20) [L^{tpy}(V$_3$POM + trizma)]$^{6-}$, 732 (20) [L^{tpy}(V$_3$POM + trizma)ClO$_4$ + H]$^{6-}$, 772 (40) [L^{tpy}(V$_3$POM + trizma)ClO$_4$ + TBA]$^{6-}$, 976 (60) [L^{tpy}(V$_3$POM + trizma)ClO$_4$ + 2TBA]$^{5-}$. IR (KBr, cm^{-1}): ν(N–H) 3458; ν(C–H)ar 3086; ν_s(CH$_3$) 2952, 2863; ν(C=O) 1644; ν(C=C)$_{ar}$ 1554; ν(C–N) 1428, 1384; ν(C=N)$_{ar}$ 1272; ρ(C–H)$_{ar}$ 1094; γ(C–H)$_{ar}$ 960, 923, 812, 752, 581, 522. ^1H NMR (400 MHz, DMSO-d_6): 8.85 ppm (s, 4H, H_L), 8.49 ppm (d, 4H, H_L), 7.97 ppm (m, 4H, H_L), 7.46 ppm (d, 4H, H_L), 5.41 ppm (s, 6H, O-CH$_2$-C), 3.17 ppm (m, 4H, H_{TBA}), 2.64 ppm (s, 12H, H_L), 1.58 ppm (m, 4H, H_{TBA}), 1.31 ppm (m, 4H, H_{TBA}), 0.94 ppm (m, 6H, H_{TBA}). ^{31}P NMR (162 MHz, DMSO-d_6): $\delta = -6.65$ ppm, -12.70 ppm.

X-ray crystallography

X-ray diffraction data were collected at 100(1) K by the ω-scan technique on Rigaku four-circle XCalibur diffractometer (Eos detector) with graphite-monochromatized MoK$_\alpha$ radiation (λ = 0.71073 Å). The data were corrected for Lorentz-polarization and absorption effects.[45] The structure was solved with SHELXT[46] and refined with the full-matrix least-squares procedure on F^2 by SHELXL.[47] Non-hydrogen atoms were refined anisotropically (*vide infra*), hydrogen atoms were placed in the calculated positions and refined as 'riding model' with the isotropic displacement parameters set at 1.2 (1.5 for methyl) times the U_{eq} value for appropriate non-hydrogen atom. The structure has been found disordered, in both ligand molecules the ethyl groups have been refined in two alternative positions, and in both cases the terminal methyl carbon atoms were left isotropic. Some constraints for C–C distances were applied. Additionally, there are regions of diffused electron density in the voids, apparently connected with the disorder solvent molecules. The attempts to model the solvent failed, so it has been refined with the SQUEEZE method.[48]

Crystal data: $(C_{40}H_{38}ZnN_6O_4)^{2+}\cdot2(ClO_4)$, M_r = 931.03, triclinic, $P\bar{1}$, a = 12.9401(8) Å, b = 13.1181(8) Å, c = 13.9436(6) Å, α = 68.923(5), β = 80.861(4), γ = 66.577(6), V = 2026.2(2) Å^3, Z = 2, d_x = 1.523 g·cm^{-3}, $F(000)$ = 958, μ = 0.743 cm^{-1}, 14 264 reflection collected, 7131 symmetry independent (R_{int} = 3.36%), 5905 with $I > 2\sigma(I)$. Final $R[I > 2\sigma(I)]$ = 0.0779, w$R_2[I > 2\sigma(I)]$ = 0.1993, R [all reflections] = 0.0928, wR_2[all reflections] = 0.2088, S = 1.102, $(\Delta\rho_{max}/\Delta\rho_{min})$ = 1.45/−0.76 e Å^{-3}. Crystallographic data for the structural analysis has been deposited with the Cambridge Crystallographic Data Centre, CCDC 2078396.†

General for biological activities

CT-DNA, Tris and NaCl were supplied from Merck and used without further purification. CT-DNA was dissolved in Tris Buffer (5 mM Tris HCl, 50 mM NaCl, pH 7.4) prior to use. The CT-DNA solution gave a ratio of UV absorbance at 260 and 280 nm and the value is lower than 1.82 : 1, indicating that the CT-DNA sample was sufficiently free from protein. CT-DNA concentration per nucleotide was determined from the UV absorbance at 260 nm using the extinction coefficient ε_{260} = 6600 dm^3 mol^{-1} cm^{-1}. Stock solutions of compounds in DMSO at concentration 2×10^{-3} M were prepared prior to use. All electronic absorption spectra were performed in 10 × 10 mm quartz cells on Jasco V-770 between 800 and 200 nm

using solutions $\sim 2 \times 10^{-5}$ M with respect to the compound concentration in Tris Buffer (5 mM Tris HCl, 50 mM NaCl, pH 7.4) with 1% DMSO content.

Stability tests

Samples were prepared by diluting aqueous stock solutions (2 mM) of compounds (25 μl) in Tris Buffer (2475 μl; 5 mM Tris HCl, 50 mM NaCl, pH 7.4). UV-Vis absorbance spectra were measured in time intervals until stabilization of spectra has been reached. The obtained data indicate that the compounds remain stable[49] and reach equilibrium within 60 minutes.

Electronic absorption titration with DNA

The absorbance titrations were performed in a fixed concentration of compounds (20 μM) while gradually increasing the concentration of CT-DNA within the range from 0 to 100 μM. Identical aliquots of CT-DNA stock solution were added to the sample and the blank solutions and a new baseline was recorded before each titration step in order to not observe the bands corresponding to CT-DNA alone in the subsequent spectra. Each sample solution was allowed to equilibrate 5 min before the spectra were recorded. Using the absorption titration data, the binding constant K_b was determined according to the equation:[50] $[DNA]/(\varepsilon_a - \varepsilon_f) = [DNA]/(\varepsilon_b - \varepsilon_f) + 1/K_b (\varepsilon_b - \varepsilon_f)$, where [DNA] is the concentration of CT-DNA in the base pairs, ε_a corresponds to the extinction coefficient observed ($A_{obsd}/[M]$), ε_f corresponds to coefficient of free compound, ε_b is the extinction coefficient of the compound fully bound to CT-DNA, and K_b is the intrinsic binding constant. The K_b value was given by the ratio of slope to intercept in the plot of $[DNA]/(\varepsilon - \varepsilon_f)$ versus [DNA].

pH driven decomposition of hybrids and electronic absorption titration of H1^{cov}, H2^{cov}, H3^{cov} with DNA in alkaline solutions

Solutions were prepared by adding stock solutions of compounds (20 μM) to MiliQ water (4 ml solution volume). The pH of each of the solutions was measured and the absorption spectra were performed by taking 2.5 ml of the solution. 2 M NaOH (1.5 μl) was then added to the test solutions to adjust the pH to alkaline. The pH of the solutions and the UV spectrum were measured. The next step was to add 100 μM CT-DNA to each sample including reference and the absorption measurement was made after 10 min, 60 min and 24 h.

Results and discussion

General rationale

WD POM hybrids with terpyridine-type ligands are known in the literature from both covalent and ionic approaches. The majority of papers focus on the covalent bonding of terpyridine ligands to WD POM, where organosilyl[51,52] or organophosphonate[53,54] functionalized WD POMs can be post-functionalized with terpyridine ligand-based complexes. In contrast, a distinct minority can be found in the literature

showing ionic bonding between WD POM and terpyridine ligand. Among the few articles, the most commonly presented is the binding of a common P_2W_{18} subunit or modified cap WD POM to a pentaerythritol-based metallodendrimer with Ru^{II} terpyridine units.[55,56]

Herein, the hybrid systems based on WD POM were obtained *via* ionic and covalent functionalization to compare if the type of POM-complex interactions affect the stability of the hybrids and whether this can be used in the presence of DNA to demonstrate the possible interactions with a simple biological system. Hybrid materials constructed *via* ionic interactions were prepared using WD POM and tridentate acyl-hydrazone N_2O ligand **L^{N2O}** with NR$_4^+$ cationic moiety and was reported by us in 2020[14] (Scheme 1b). The simplicity of the system lies in the fact that WD counterpart is non-functionalized, easily available and its highly negative charge is responsible for interactions with ligand **L^{N2O}** or its complexes, ultimately forming (CD)-SEC materials. Please note that it was previously demonstrated in the literature that introduction of the cationic moiety in the acyl-hydrazone group can influence the binding propensy of the system to the DNA.[57] These hybrid materials termed **H1^{ion}–H3^{ion}** are studied for their interactions with DNA (see Section: interaction of ionic hybrids with DNA). Herein, we constructed new class of WD hybrid materials based on the inorganic WD POM and 6,6″-dimethyl-2,2′:6′,2″-terpyridine-type ligand **L^{tpy}**, which is based on the covalent functionalization. Tris(hydroxymethyl)aminomethane (TRIZMA) was chosen as the anchoring group, given its wide and successful utilization in the POM chemistry.[58]

Onto the TRIZMA-modified mono-substituted WD POM (**V$_3$POM + TRIZMA**), **L^{tpy}** ligand was chemically grafted through the ester group in the *p*-position of the central tpy N-heterocyclic ring (Scheme 1c). We have previously demonstrated that the methylated version of the tpy ligand can efficiently form bimetallic $[Ag_2L_2]^{2+}$ helicates, which demonstrated cytotoxic character towards chosen cancer cell lines,[59] hence we envisaged that the formed POM covalent hybrids **H1^{cov}–H3^{cov}** have the potential to exhibit related properties and therefore interaction with DNA were studied and compared with **H1^{ion}–H3^{ion}** materials. Please note that irrespectively of the chosen type of connection (ionic or covalent), **H1** denotes POM-ligand hybrid, whereas **H2** and **H3** its complex with zinc(II) chloride and perchlorate, respectively.

Synthetic considerations for substrates

The synthetic pathway was divided into independent groups: preparation of TRIZMA-functionalized Wells–Dawson system **V$_3$POM + TRIZMA** (Scheme 1a), synthesis of ligand **L^{tpy}** and its two zinc(II) complexes **K1** [Zn(**L^{tpy}**)Cl$_2$], **K2** [Zn(**L^{tpy}**)$_2$](ClO$_4$)$_2$ (Scheme 1e). After preparing the precursors, the synthesis of the seven hybrid materials **H1^{cov}–H7^{cov}** was carried out using different routes (Scheme 1c). Details, including synthetic procedures and characterization are included in the Experimental section and ESI,† respectively.

The general procedure (Scheme 1a) involves selective lacunarization of the parent K$_6$[P$_2$W$_{18}$O$_{62}$] WD POM and
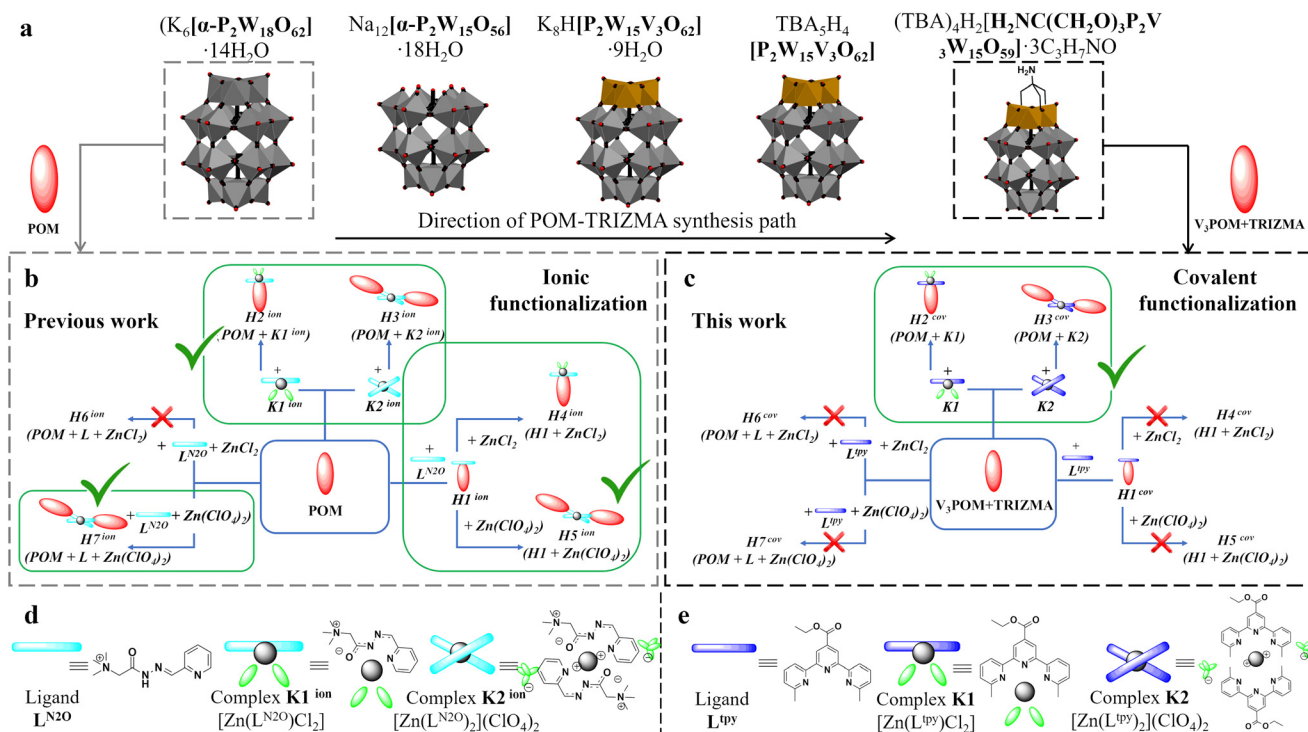
Scheme 1 (a) Scheme of synthesis path of WD POM in their polyhedral representations; schematic representation of hybrids constructed *via* (b) ionic[14] and (c) covalent interactions; schematic representation structures of (d) ligand L^{N2O} and complexes $K1^{ion}$ [Zn(L^{N2O})Cl$_2$], $K2^{ion}$ [Zn(L^{N2O})$_2$](ClO$_4$)$_2$, respectively; and (e) ligand L^{tpy} [C$_{20}$H$_{19}$N$_3$O$_2$] and complexes $K1$ [Zn(L^{tpy})Cl$_2$], $K2$ [Zn(L^{tpy})$_2$](ClO$_4$)$_2$, respectively.

subsequent implementation of the vanadium cap, which renders the system prone to selective integration of the TRIZMA linker. Such amino-functionalized POM allows one to graft the tpy ligand in a robust, covalent manner through the amide bond, which was demonstrated to be feasible approach.[60,61]

Ligand L^{tpy} was obtained according to the slightly modified reported procedure[44] *via* the Stille coupling protocol (Scheme S1†) and was used for complexation reactions with ZnCl$_2$ and Zn(ClO$_4$)$_2$, thus allowing formation of complexes $K1$ [Zn(L^{tpy})Cl$_2$] and $K2$ [Zn(L^{tpy})$_2$](ClO$_4$)$_2$, respectively. In both cases, the reaction was conducted in a mixture of methanol/ acetonitrile (1 : 1, v : v) for 24 hours at room temperature. The purity of the compound and the repeatability of the desired product were confirmed by ESI-MS, elementary analysis, FT-IR, ^{1}H NMR and ^{31}P NMR spectroscopy are described in detail in the Experimental section and ESI.† X-ray crystal structure of complex $K2$ is described in Section: X-ray crystal characterization of complex $K2$.

X-ray crystal characterization of complex K2

Fig. 1a shows the perspective view of the [Zn(L^{tpy})$_2$]$^{2+}$ cation in structure $K2$. The Zn^{II} ion is 6-coordinated, by six nitrogen atoms – three from each ligand molecule. The coordination might be described as distorted octahedral, with the Zn–N distances within the range 2.054(5) Å–2.311(4) Å, and the three largest.
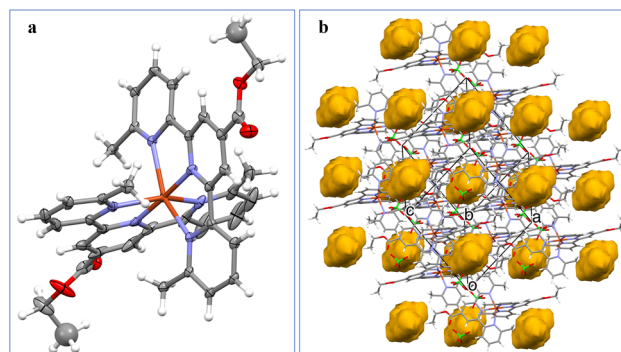

Fig. 1 (a) Perspective view of the dicationic complex $K2$ [Zn(L^{tpy})$_2$]$^{2+}$; (b) the ellipsoids are drawn at the 30% probability level, hydrogen atoms are represented by spheres of arbitrary radii.

N–Zn–N angles equal 176.17(17)°, 151.07(19)°, and 151.63 (15)°. The crystal architecture is determined mainly be electrostatic interactions between charged species; there are voids filled with diffused electron density (Fig. 1b).

Synthesis and characterization of hybrid materials

The obtained precursors, both $V_3POM + TRIZMA$, ligand L^{tpy} and Zn(II) complexes $K1$ and $K2$, were reacted to obtain three distinct families of hybrid materials $H1^{cov}$–$H3^{cov}$ ($H1^{cov}$ – POM with grafted ligand; $H2^{cov}$ – POM with grafted complex $K1$; $H3^{cov}$ – POM with grafted complex $K2$) that can be potentially

formed *via* seven different routes – depicted in Scheme 1c. Since we observed in our previous study[14] that not every route is feasible for the construction of ionic assemblies $H1^{ion}$– $H3^{ion}$, the same approach needs to be performed for the covalent class. Please note that for clarity purposes, each process was termed as $H1^{cov}$–$H7^{cov}$, where $H1^{cov}$–$H3^{cov}$ denote reactions of POM with ligand L^{tpy} or its complexes; $H4^{cov}$ and $H5^{cov}$ denote reaction of $H1^{cov}$ with metal salts (so called step-by-step approach) and $H6^{cov}$ and $H7^{cov}$ denote one-pot reaction of all substrates (POM, L^{tpy} and metal ion salts).

Synthesis of $H1^{cov}$–$H3^{cov}$ hybrids

Synthesis of hybrids of $H1^{cov}$–$H3^{cov}$ through direct reaction of amino-functionalized WD POM synthesis with L^{tpy} ($H1^{cov}$) or its zinc complexes $K1$ ($H2^{cov}$) and $K2$ ($H3^{cov}$) was performed through heating of substrates under reflux and successfully confirmed by a series of analytical methods (ESI-MS, elementary analysis, FT-IR, ^{1}H NMR spectroscopy, ^{31}P NMR spectroscopy) and is described in detail in the Experimental section and ESI.† Comparison of ^{1}H NMR spectra of respective substrates and their products ($H1^{cov}$ – Fig. S24 and S25; $H2^{cov}$ – Fig. S26 and S27; $H3^{cov}$ – Fig. S28 and S29†) shows changes that are consistent with covalent bonding of the organic counterparts with the inorganic POM core (see also Fig. 2 of the aromatic region). FT-IR spectra (Fig. S4–S6†) also confirm the conducted reactions *via* the NH and C=O frequency shifts but importantly, together with ^{31}P NMR (Fig. S40–S42†) confirms that the WD POM retained its structural integrity. ESI-MS analyses also prove formation of the desired products. Interestingly, while the sole complex $K1$ shows the ^{1}H NMR signature of the solution speciation between the 1:1 M:L $[Zn(L^{tpy})Cl_2]$ and the 1:2 M:L $[Zn(L^{tpy})_2]^{2+}$ complexes – which is also observed in the literature for other tpy systems[62] – the $H2^{cov}$ hybrid does not exhibit such a character. The nBu_4N^+ cations inherent to the negatively charged POM species are also observed in the hybrid materials and integrated accordingly (6 for $H1^{cov}$ and $H2^{cov}$, 12 for $H3^{cov}$ hybrid). These were demonstrated to be inter-exchangeable,[63] which provides additional means for future functionalization.

Synthesis of $H4^{cov}$ and $H5^{cov}$ hybrids

Synthesis of $H4^{cov}$ and $H5^{cov}$ hybrids was anticipated to form analogues of $H2^{cov}$ and $H3^{cov}$ hybrids respectively, attempted from $H1^{cov}$ hybrid *i.e.* system with L^{tpy} ligand covalently grafted onto the WD POM. While changes indicative of the molecular transformations were observed during the synthetic procedure, the isolation and characterization of hybrids ($H4^{cov}$ – Fig. S7, S18, S30, S31 and S43; $H5^{cov}$ – Fig. S8, S19, S32, S33 and S44†) showed that $ZnCl_2$ and $Zn(ClO_4)_2$ salts are not readily coordinated in the tpy pocket, but lead to partial hydrolysis resulting in the exchange of nBu_4N^+ counteractions for the acidic protons – partial in the case of $H4^{cov}$ ($2H^+$ and $4nBu_4N^+$ remain ionically bound to the POM hybrid) and complete in the case of $H5^{cov}$ ($12H^+$ and no nBu_4N^+ cations). What needs to be noted is the fact that in both cases the covalently bound tpy ligand remained grafted on the POM cluster and the polyoxometalate remained its plenary character. This is interesting, given the fact that in the presence of ionic hybrids,[14] we did observe the possibility of retrieving $H2^{ion}$ and $H3^{ion}$ analogues *via* this synthetic route to the certain extent ($H3^{ion}$ perchlorates being more stable than the $H2^{ion}$ chloride analogues) and that $H1^{ion}$ hybrid was ultimately the most stable system.

Synthesis of $H6^{cov}$ and $H7^{cov}$ hybrids

Synthesis of $H6^{cov}$ and $H7^{cov}$ hybrids was expected to form analogues of $H2^{cov}$ and $H3^{cov}$ hybrids, respectively, attempted in the form of the one-pot reaction *i.e.* from which means combination of both POM, ligand L^{tpy} and appropriate $Zn(II)$ salt in one vessel. Isolation and characterization of products ($H6^{cov}$ – Fig. S9, S20, S34, S35 and S45; $H7^{cov}$ – Fig. S10, S21, S36, S37 and S46†) and comparison with previously synthesized samples (Fig. S38, S39 and S47†) allowed us to establish that covalent grafting of the tpy ligand was successful (per analogy to the $H1^{cov}$ hybrid) and zinc(II) cations did not coordinate to the N_3 tridentate pocket but resulted in an almost complete counterion exchange from nBu_4N^+ cations to the acidic protons ($H6^{cov}$ – $TBA_{(6-x)}H_x$; $x = 5.75$; $H7^{cov}$ – $TBA_{(12-x)}H_x$; $x = 11.5$). This further confirms that in order for the covalent WD hybrids to retain $Zn(II)$ ions in their molecular composition, one has to use the preformed complexes in the form of $K1$ or $K2$ compounds. As in previous instances, integrity of the WD POM counterpart was confirmed *via* ^{31}P NMR (Fig. S47†). The remarkable stability of the $H1^{cov}$ and $H1^{ion}$ (previously demonstrated[14]) hybrids combined with excellent water solubility led us to focus on the domain of bioassays.

Biological activities – general considerations

Polyoxometalates,[64,65] organic multidentate ligands and their $Zn(II)$ complexes[57,66,67] were demonstrated in the literature to exhibit promising biological properties. Utilization of such
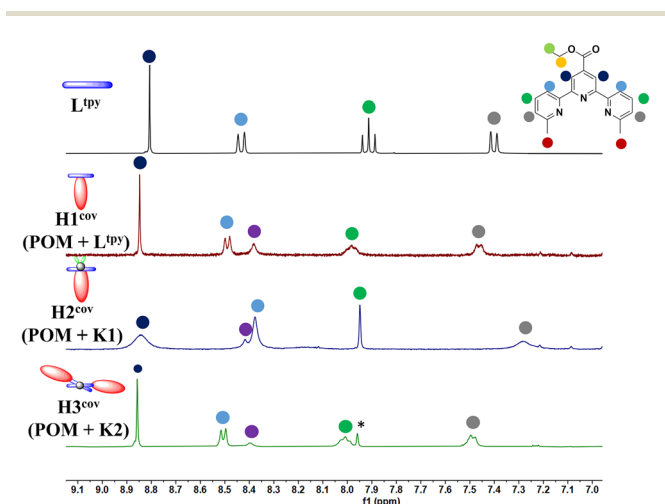

Fig. 2 Comparison of aromatic region of ^{1}H NMR spectra of L^{tpy} and hybrids: $H1^{cov}$, $H2^{cov}$ and $H3^{cov}$ in d^6-DMSO. Counterions are omitted for clarity.

materials in bioassays significantly depends on the functionalization method and stability of the system, yet these aspects were very scarcely studied in hybrid materials based on WD POM scaffold and remain unknown, and only relatively recently such a niche was highlighted upon the fact that organic functionalization of the POM inorganic clusters alleviates some of the drawbacks that are inherent to the sole POM within the context of biotoxicity.[24] One of the primary cellular targets of drugs in cancer cells is the DNA present in the nuclei. Owing to the large size and the negative charge of both unfunctionalized POMs and DNA assemblies they are expected to rather repulse than interact between each other. It was however demonstrated that functionalization of POM clusters may reverse this trend or at least provide an alternative interaction path. For instance, Wang and co-workers[68] have reported cyclopentadienyltitanium substituted polyoxotungstate $[CoW_{11}O_{39}(CpTi)]^{7-}$ (Cp = η^5-C_5H_5) that is able to cleave the supercoiled DNA macrostructure. In addition, Dianat *et al.*[69] showed $K_6H[CoW_{11}O_{39}CpZr]$, $K_6H[CoW_{11}O_{39}CpTi]$ and $K_7H_2[CoW_{11}O_{39}CpFe]$ Keggin-type POMs, that tend to interact with the phosphate backbone of the DNA *via* electrostatic interactions.

Herein, we aimed to elucidate the affinity of the hybrid compounds (ionic **Hx^ion** *vs.* covalent **Hx^cov**) toward CT-DNA (deoxyribonucleic acid sodium salt from calf thymus), a model reagent used for routine DNA studies.[70] Since the electrostatic character of **Hx^ion**–**H1** (neutral), **H2** (anionic) and **H3** (anionic) is structure dependent, the interplay between them and DNA scaffold may be dissimilar to those previously described. At the same time, covalent functionalization of the POM hybrid can also be anticipated to help, especially since we did demonstrate previously that the silver(I) helical complexes of the related tpy ligand bind nucleic acids.[59] Both types of hybrids reach equilibrium within *ca.* 60 min and remain stable in the buffered medium (Fig. S48 and S49†).[49] Therefore, in order to probe the interactions between the synthesized hybrid materials **H1^ion**, **H2^ion**, **H3^ion**, **H1^cov**, **H2^cov**, **H3^cov** and also the corresponding complexes with the nucleic acid, a solution of the corresponding compound was titrated with CT-DNA samples.

Interaction of ionic hybrids with DNA

Significant changes in the shape of the spectra were observed for a series of CD-SEC hybrids **H2^ion** and **H3^ion**, contrary to the **H1^ion** system, which remained unchanged (Fig. 3 and Fig. S50†). In particular, the MLCT bands at 345 nm for **H2^ion** and 339 nm for **H3^ion** characteristic for the CD-SEC entities disappeared. Simultaneously, new bands, peculiar for **H1^ion**, at 257 nm and 290 nm appear. We surmise that this means that **H2^ion** and **H3^ion** undergo a structural transformation to **H1^ion** in the presence of DNA (compare Fig. 3) with the binding constant K_b of 2.5×10^5 M^{-1} (Fig. S50†) through decomplexation mechanism. Further experiments confirmed that the substrate complexes **K1^ion** and **K2^ion**, in fact, interact with DNA what is manifested by the moderately high binding constants of K_b = 6.7×10^4 and 1.2×10^5 M^{-1}, respectively (Fig. S51†). In case of

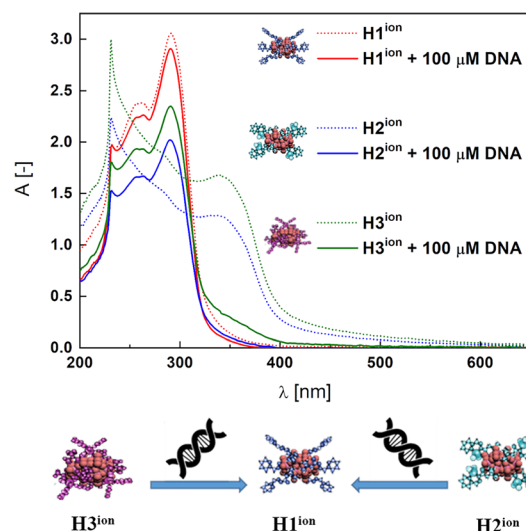**Fig. 3** **H1^ion**, **H2^ion** and **H3^ion** alone and the effect of CT-DNA addition.

both complexes, a hypsochromic shifts of *ca.* 10 nm of ILCT bands (*ca.* 295 nm) were observed. Changes in the intensity and position of the ligand-derived bands may suggest electrostatic interaction with CT-DNA. On the other hand, isosbestic points at *ca.* 305 nm as well as hypochromism of MLCT bands at *ca.* 345 nm are present and, together with the reported K_b values, indicate binding to DNA, possibly, by intercalation.[71,72] This indicates that the **H2^ion** and **H3^ion** are able to rearrange themselves to **H1^ion**. It also highlights the stability of the **H1^ion** in a cellular-like environment, making it a potential drug delivery platform.

Potential drugs such as platinum complexes[73] bound in SEC system as CD-SEC systems may be released in the presence of cellular DNA and then interact with its backbone *via* covalent binding thus inhibiting the cells vital processes as replication and transcription.

Interaction of covalent hybrids with DNA

It should be noted that in order to gain a deeper insight into the nature of the counterions present in the system and the changes associated to the POM transformations (Scheme 1a), a much larger number of substrates were tested for stability – including the V_3-capped WD POM with varying countercations (K^+ (**V_3POM-K8**), nBu_4N^+ (**V_3POM-TBA**), nBu_4N^+ functionalized with TRIZMA (**V_3POM + trizma**)), including the **L^tpy** ligand and its **K2** complex (**K1** is very poorly soluble in aqueous media). It occurred that functionalization of the WD POM with TRIZMA renders the system more stable that its non-substituted counterparts **V_3POM-K8** and **V_3POM-TBA** (Fig. S49†).

The covalently linked **H1^cov**–**H3^cov** hybrids did not bind to the DNA scaffold (Fig. S51†). However, the substrate ligand **L^tpy** and **K2** complex easily bound to DNA what is reflected in the high binding constants, respectively, 2.6×10^6 M^{-1} and 1.1×10^5 M^{-1} (Fig. 4 and Fig. S52†).
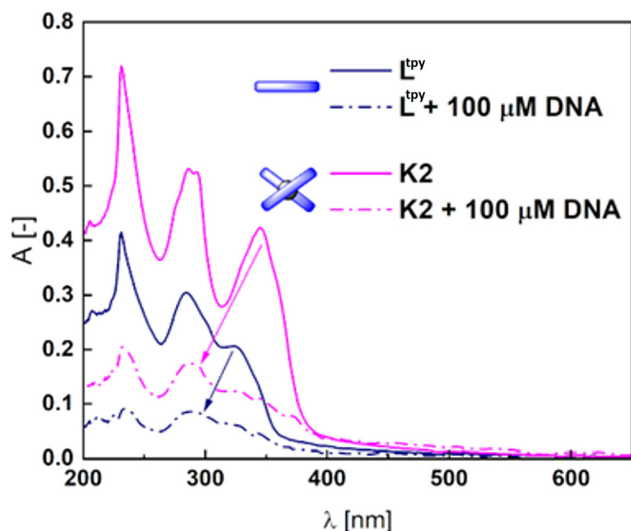
Fig. 4 L^{tpy} and **K2** alone and the effect of CT-DNA addition. Arrows indicate the trend of changes.

Fig. 5 $H1^{cov}$, $H2^{cov}$ and $H3^{cov}$ alone in miliQ water (starting pH *ca.* 5.9) and the effect of basification (up to pH $\sim$ 8.6) and CT-DNA addition. Scheme below – schematic illustration using the example of $H2^{cov}$ of pH dependent hydrolysis leading to the breakdown into basic inorganic building subunits.

Addition of DNA to both compounds caused significant hypochromic changes in the spectra implying the intercalation.[71,72] **K1** complex is insoluble in buffer with DMSO, therefore the K_b was not calculated. However, its derivatization with POM increased its solubility (Fig. S52†) and the structure similarity to L^{tpy} and **K2** allows to surmise it could interfere with the DNA after the exchange of monovalent ligands. The stability of $H1^{cov}$–$H3^{cov}$ hybrids in acidic (*cf.* synthesis) and normal cellular pH (7.4) opens a path to a controlled release of the ligand and complexes in basic pH in the duodenum and small intestine (pH $\sim$ 8). Basification of the acidic solutions of $H1^{cov}$–$H3^{cov}$ (*ca.* 5.9) to pH $\sim$ 8.2–8.6 led to some morphological changes within 1 h in the UV spectra indicating slow decomposition of the hybrids in the POM region[63] (Fig. 5 and Fig. S53†). Then, to the partially decomposed covalent hybrids, the DNA was added and some subtle changes in the band's intensity were detected (Fig. 5 and Fig. S53†). One can observe that the $H2^{cov}$ is more readily decomposed than $H3^{cov}$ probably due to the insolubility of **K1** and the lower stability of the complexes of 1:1 ligand:metal ratio in comparison to 2:1 complexes as **K2**. We find it as evidence for the facilitation of the DNA binding process, possibly, due to the detaching of the POM octahedrons.[63,74] Changes are less abrupt that in the case of Hx^{ion} hybrids (Fig. 3).

This means that depending on the character of the chosen hybrid (covalent *vs.* ionic) one can envisage those systems to become cargo-loading drug candidates, with functionalization mode ultimately affecting the stability and eventual pharmacotherapeutic effect – which was demonstrated for the anchored organic ligand/complex (interaction constant K_b = 2.5×10^5 M^{-1}, insets in Fig. S50†). The ultimate mechanism is however different; for Hx^{ion} hybrids, the ionic interactions make it very fast system, where POM remains intact in its $H1^{ion}$ form and the disturbance of ionic interactions results in
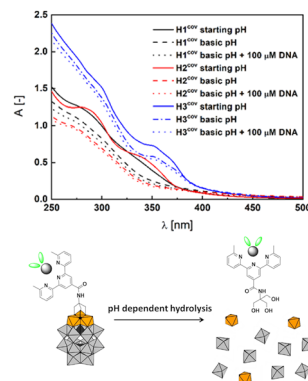
cargo-release of the appended molecules; for Hx^{cov} hybrids the POM hydrolyses through the pH dependent mechanisms, therefore ligand/complex is released together with disintegration of WD POM into the basic inorganic building subunits (Fig. 4).

Conclusions

In summary, we have presented the effect of various synthetic methods on the synthesis of three different families of $H1^{cov}$–$H3^{cov}$ hybrid materials. The first synthetic method involved the reaction of POM with the ligand L^{tpy} or its complexes: **K1** or **K2**; the second synthetic method involved the reaction of $H1^{cov}$ with metal salts (step-by-step approach), and the third involved the reaction between POM, L^{tpy} and metal ion salts (one-pot approach). As a result, the desired hybrid materials were obtained using the first synthetic method and we have demonstrated for the first time how hybrid materials based on Wells–Dawson Polyoxometalates interact with DNA and how their functionalization mode (ionic/covalent) modulates the stability of the hybrid and the extent of DNA binding. This was done by comparing the ionic Hx^{ion} hybrids synthesized previously[14] and newly prepared covalent Hx^{cov} hybrids. Protocols for the latter ones were also developed, giving therefore different means for their functionalization and demonstrating which molecular parts of the hybrids are amenable to further synthetic changes. Specifically, the acidic character of the zinc(II) salts is responsible for part of those transformations.

In the presence of DNA, the synthesized ionic and covalent hybrids undergo reorganizations, which in both instances lead to the release of the bound ligands/complexes, nonetheless the ultimate mechanism is different. For Hx^{ion} ionic hybrids, fast elimination of the coordinated zinc(II) ions/ligands from $H2^{ion}$ and $H3^{ion}$ hybrids is observed, concomitant with transformation to the $H1^{ion}$ hybrid due to the significant stability of the latter one. For Hx^{cov} covalent hybrids, slow pH mediated hydro-

lysis of the polyoxometalate was observed, which leads to release of the grafted ligand/complex to the surrounding aqueous medium. High binding constant of terpyridine ligand and its complex $[Zn(L^{tpy})_2](ClO_4)_2$ to the DNA was also demonstrated. This overall shows that the WD POM has the potential to act as the cargo-loading system, which we anticipate to study further.

Author contributions

Daria Nowicka: investigation, methodology, formal analysis, data curation, visualization, writing – review & editing, funding acquisition. Dawid Marcinkowski: investigation, methodology, formal analysis, data curation, visualization, writing – review & editing, funding acquisition. Nahir Vadra: investigation, methodology, formal analysis, data curation, visualization, writing – review & editing. Martyna Szymańska: investigation, methodology, formal analysis, data curation, visualization, writing – review & editing. Maciej Kubicki: formal analysis, investigation, data curation, writing – review & editing, visualization. Giuseppe Consiglio: conceptualization, visualization, writing – review & editing. Wojciech Drożdż: investigation, formal analysis, data curation, writing – review & editing. Artur R. Stefankiewicz: resources, visualization, writing – review & editing. Violetta Patroniak: supervision, resources, writing – review & editing, funding acquisition. Marta Fik-Jaskółka: investigation, conceptualization, methodology, writing – review & editing, project administration, supervision, resources, funding acquisition. Adam Gorczyński: conceptualization, methodology, writing – review & editing, project administration, supervision, resources.

Conflicts of interest

There are no conflicts to declare.

Acknowledgements

References

1 D.-L. Long, R. Tsunashima and L. Cronin, *Angew. Chem., Int. Ed.*, 2010, **49**, 1736–1758.

2 S. Lentink, D. E. Salazar Marcano, M. A. Moussawi and T. N. Parac-Vogt, *Angew. Chem., Int. Ed.*, 2023, **62**, e202303817.

3 X.-K. Lian, H.-B. Chen, Y.-D. Lin, X.-X. Li and S.-T. Zheng, *Coord. Chem. Rev.*, 2023, **497**, 215440.

4 L. Vilà-Nadal and L. Cronin, *Nat. Rev. Mater.*, 2017, **2**, 17054.

5 L. Cronin, *Ann. Rep. Prog. Chem., Sect. A: Inorg. Chem.*, 2004, **100**, 323–383.

6 L.-L. Liu, L. Wang, X.-Y. Xiao, P. Yang, J. Zhao and U. Kortz, *Coord. Chem. Rev.*, 2024, **506**, 215687.

7 A. Misra, K. Kozma, C. Streb and M. Nyman, *Angew. Chem., Int. Ed.*, 2020, **59**, 596–612.

8 H. N. Miras, J. Yan, D.-L. Long and L. Cronin, *Chem. Soc. Rev.*, 2012, **41**, 7403–7430.

9 V. Duros, J. Grizou, W. Xuan, Z. Hosni, D.-L. Long, H. N. Miras and L. Cronin, *Angew. Chem., Int. Ed.*, 2017, **56**, 10815–10820.

10 D. S. Salley, G. A. Keenan, D. L. Long, N. L. Bell and L. Cronin, *ACS Cent. Sci.*, 2020, **6**, 1587–1593.

11 A. V. Anyushin, S. Vanhaecht and T. N. Parac-Vogt, *Inorg. Chem.*, 2020, **59**, 10146–10152.

12 Q. Liu and X. Wang, *Matter*, 2020, **2**, 816–841.

13 A. Dolbecq, E. Dumas, C. R. Mayer and P. Mialane, *Chem. Rev.*, 2010, **110**, 6009–6048.

14 A. Bocian, W. Drożdż, M. Szymańska, J. Lewandowski, M. Fik-Jaskółka, A. Gorczyński, V. Patroniak and A. R. Stefankiewicz, *Nanoscale*, 2020, **12**, 4743–4750.

15 S.-S. Wang and G.-Y. Yang, *Chem. Rev.*, 2015, **115**, 4893–4962.

16 S. Li, Y. Ma, Y. Zhao, R. Liu, Y. Zhao, X. Dai, N. Ma, C. Streb and X. Chen, *Angew. Chem., Int. Ed.*, 2023, **62**, e202314999.

17 M. Yang, X. Wang, C. J. Gómez-García, Z. Jin, J. Xin, X. Cao, H. Ma, H. Pang, L. Tan, G. Yang and Y. Kan, *Adv. Funct. Mater.*, 2023, **33**, 2214495.

18 X. Chen, C. Ma, Z. Tan, X. Wang, X. Qian, X. Zhang, J. Tian, S. Yan and M. Shao, *Chem. Eng. J.*, 2022, **433**, 134504.

19 J.-J. Chen, M. D. Symes and L. Cronin, *Nat. Chem.*, 2018, **10**, 1042–1047.

20 A. Bijelic and A. Rompel, *Acc. Chem. Res.*, 2017, **50**, 1441–1448.

21 Y. Martinetto, B. Pégot, C. Roch-Marchal, B. Cottyn-Boitte and S. Floquet, *Eur. J. Inorg. Chem.*, 2020, **2020**, 228–247.

22 S.-M. Wang, J. Hwang and E. Kim, *J. Mater. Chem. C*, 2019, **7**, 7828–7850.

23 U. Kortz, A. Müller, J. van Slageren, J. Schnack, N. S. Dalal and M. Dressel, *Coord. Chem. Rev.*, 2009, **253**, 2315–2327.

24 J. T. Rhule, C. L. Hill, D. A. Judd and R. F. Schinazi, *Chem. Rev.*, 1998, **98**, 327–358.

25 B. Hasenknopf, *Front. Biosci.*, 2005, **10**, 275–287.

26 M. Arefian, M. Mirzaei, H. Eshtiagh-Hosseini and A. Frontera, *Dalton Trans.*, 2017, **46**, 6812–6829.

27 T. Liu, *Langmuir*, 2010, **26**, 9202–9213.

28 P. Gao, Y. Wu and L. Wu, *Soft Matter*, 2016, **12**, 8464–8479.

29 S. Vanhaecht, G. Absillis and T. N. Parac-Vogt, *Dalton Trans.*, 2012, **41**, 10028–10034.

30 K.-i. Shimizu, H. Furukawa, N. Kobayashi, Y. Itaya and A. Satsuma, *Green Chem.*, 2009, **11**, 1627–1632.

31 J. Zhang, *Trends in Polyoxometalates Research*, 2015.

32 A. Flütsch, T. Schroeder, M. G. Grütter and G. R. Patzke, *Bioorg. Med. Chem. Lett.*, 2011, **21**, 1162–1166.

33 K. Nomiya, H. Torii, T. Hasegawa, Y. Nemoto, K. Nomura, K. Hashino, M. Uchida, Y. Kato, K. Shimizu and M. Oda, *J. Inorg. Biochem.*, 2001, **86**, 657–667.

34 A. Bijelic, M. Aureliano and A. Rompel, *Chem. Commun.*, 2018, **54**, 1153–1169.

35 A. Bijelic, M. Aureliano and A. Rompel, *Angew. Chem., Int. Ed.*, 2019, **58**, 2980–2999.

36 L. Fu, H. Gao, M. Yan, S. Li, X. Li, Z. Dai and S. Liu, *Small*, 2015, **11**, 2938–2945.

37 D. Li, P. Yin and T. Liu, *Dalton Trans.*, 2012, **41**, 2853–2861.

38 X. Wang, J. Liu and M. Pope, *Dalton Trans.*, 2003, 957–960.

39 S. K. Petrovskii, E. V. Grachova and K. Y. Monakhov, *Chem. Sci.*, 2024, **15**, 4202–4221.

40 R. Contant and A. Tézé, *Inorg. Chem.*, 1985, **24**, 4610–4614.

41 B. J. Hornstein and R. G. Finke, *Inorg. Chem.*, 2002, **41**, 2720–2730.

42 R. G. Finke, B. Rapko, R. J. Saxton and P. J. Domaille, *J. Am. Chem. Soc.*, 1986, **108**, 2947–2960.

43 C. P. Pradeep, D.-L. Long, G. N. Newton, Y.-F. Song and L. Cronin, *Angew. Chem., Int. Ed.*, 2008, **47**, 4388–4391.

44 G. Ulrich, S. Bedel, C. Picard and P. Tisnès, *Tetrahedron Lett.*, 2001, **42**, 6113–6115.

45 *CrysAlis PRO (Version 1.171.38.41)*, 2015.

46 G. M. Sheldrick, *Acta Crystallogr., Sect. A: Found. Adv.*, 2015, **71**, 3–8.

47 G. M. Sheldrick, *Acta Crystallogr., Sect. C: Struct. Chem.*, 2015, **71**, 3–8.

48 A. L. Spek, *Acta Crystallogr., Sect. C: Struct. Chem.*, 2015, **71**, 9–18.

49 J. Skiba, T. Bernaś, D. Trzybiński, K. Woźniak, G. Ferraro, D. Marasco, A. Merlino, M. Z. Shafikov, R. Czerwieniec and K. Kowalski, *Molecules*, 2017, **22**, 809.

50 L. Shivakumar, K. Shivaprasad and H. D. Revanasiddappa, *Spectrochim. Acta, Part A*, 2012, **97**, 659–666.

51 G. Izzet, B. Abécassis, D. Brouri, M. Piot, B. Matt, S. A. Serapian, C. Bo and A. Proust, *J. Am. Chem. Soc.*, 2016, **138**, 5093–5099.

52 B. Matt, C. Coudret, C. Viala, D. Jouvenot, F. Loiseau, G. Izzet and A. Proust, *Inorg. Chem.*, 2011, **50**, 7761–7768.

53 E. Hampson, J. M. Cameron, S. Amin, J. Kyo, J. A. Watts, H. Oshio and G. N. Newton, *Angew. Chem.*, 2019, **131**, 18449–18453.

54 E. Hampson, J. M. Cameron, J. A. Watts and G. N. Newton, *Chem. Commun.*, 2020, **56**, 8237–8240.

55 M. Zynek, M. Serantoni, S. Beloshapkin, E. Dempsey and T. McCormac, *Electroanalysis*, 2007, **19**, 681–689.

56 R. I. Nooney, D. Thirunavukkarasu, Y. Chen, R. Josephs and A. E. Ostafin, *Chem. Mater.*, 2002, **14**, 4721–4728.

57 W. Drożdż, A. Walczak, Y. Bessin, V. Gervais, X.-Y. Cao, J.-M. Lehn, S. Ulrich and A. R. Stefankiewicz, *Chem. – Eur. J.*, 2018, **24**, 10802–10811.

58 A. V. Anyushin, A. Kondinski and T. N. Parac-Vogt, *Chem. Soc. Rev.*, 2020, **49**, 382–432.

59 M. A. Fik, A. Gorczyński, M. Kubicki, Z. Hnatejko, A. Fedoruk-Wyszomirska, E. Wyszko, M. Giel-Pietraszuk and V. Patroniak, *Eur. J. Med. Chem.*, 2014, **86**, 456–468.

60 A. Proust, B. Matt, R. Villanneau, G. Guillemot, P. Gouzerh and G. Izzet, *Chem. Soc. Rev.*, 2012, **41**, 7605–7622.

61 M. Najafi, *ChemCatChem*, 2023, **15**, e202201045.

62 M. Wałęsa-Chorab, A. R. Stefankiewicz, D. Ciesielski, Z. Hnatejko, M. Kubicki, J. Kłak, M. J. Korabik and V. Patroniak, *Polyhedron*, 2011, **30**, 730–737.

63 D. E. Salazar Marcano, S. Lentink, M. A. Moussawi and T. N. Parac-Vogt, *Inorg. Chem.*, 2021, **60**, 10215–10226.

64 N. I. Gumerova and A. Rompel, *Inorg. Chem.*, 2021, **60**, 6109–6114.

65 L. S. Van Rompuy and T. N. Parac-Vogt, *Curr. Opin. Biotechnol.*, 2019, **58**, 92–99.

66 W. Drożdż, Y. Bessin, V. Gervais, X. Y. Cao, J. M. Lehn, A. R. Stefankiewicz and S. Ulrich, *Chem. – Eur. J.*, 2018, **24**, 1518–1521.

67 F. Nachon, X. Brazzolotto, J. Dias, C. Courageux, W. Drożdż, X.-Y. Cao, A. R. Stefankiewicz and J.-M. Lehn, *ChemBioChem*, 2022, **23**, e202200456.

68 X. Wang, J. Liu, J. Li, Y. Yang, J. Liu, B. Li and M. T. Pope, *J. Inorg. Biochem.*, 2003, **94**, 279–284.

69 S. Dianat, A. K. Bordbar, S. Tangestaninejad, B. Yadollahi, S. H. Zarkesh-Esfahani and P. Habibi, *J. Photochem. Photobiol., B*, 2013, **124**, 27–33.

70 M. Szymańska, M. Kubicki, G. N. Roviello, G. Consiglio, M. A. Fik-Jaskółka and V. Patroniak, *Dalton Trans.*, 2022, **51**, 15648–15658.

71 S. Tabassum, S. Amir, F. Arjmand, C. Pettinari, F. Marchetti, N. Masciocchi, G. Lupidi and R. Pettinari, *Eur. J. Med. Chem.*, 2013, **60**, 216–232.

72 A. A. Almaqwashi, T. Paramanathan, I. Rouzina and M. C. Williams, *Nucleic Acids Res.*, 2016, **44**, 3971–3988.

73 S. Ghosh, *Bioorg. Chem.*, 2019, **88**, 102925.

74 N. I. Gumerova and A. Rompel, *Chem. Soc. Rev.*, 2020, **49**, 7568–7601.